ACS APPLIED MATERIALS & INTERFACES

Research Article

www.acsami.org

Solution-Processable Triindoles as Hole Selective Materials in Organic Solar Cells

Steve W. Shelton,[†,‡,§] Teresa L. Chen,[†,§] David E. Barclay,[†] and Biwu Ma*[,†]

[†]The Molecular Foundry, Lawrence Berkeley National Laboratory, Berkeley, California 94720, United States

[‡]Department of Materials Science and Engineering, University of California, Berkeley, California 94720, United States

Supporting Information

ABSTRACT: We report the use of two solution-processable triindoles, triazatruxene (TAT), and N-trimethyltriindole (TMTI), as hole selective materials in organic solar cells. The unique optical and electronic properties of these molecules make them suitable as a hole extracting/electron blocking layer, i.e. transparency in the visible region due to a wide bandgap, high LUMO (lowest unoccupied molecular orbital) energy level, modest HOMO (highest occupied molecular orbital) level, and high hole carrier mobility. TAT is shown to have a LUMO at −1.68 eV, a HOMO at −5.03 eV, and a bandgap of 3.35 eV, whereas TMTI has a LUMO at −2.05 eV, a HOMO at −5.1 eV, and a bandgap of 3.05 eV, obtained from cyclic voltammetry measurements and absorption spectroscopy. Planar heterojunction photovoltaic devices, consisting of a solution processed transparent TAT (or TMTI) layer and a vapor-deposited C60 layer, exhibited efficiencies of up to 0.71 % (or 0.87 %). In these bilayer devices, the excitons are primarily generated in the C60 layer and undergo dissociation in the interfaces via hole transfer from the C60 layer to the TAT (or TMTI) layer. Additionally, spin-casting methanol solution of TAT on the top of P3HT:PCBM bulk heterojunction in an inverted device produced a hole selective interfacial layer between the photoactive layer and anode, leading to a 26% efficiency increase as compared to a control device without the TAT layer.

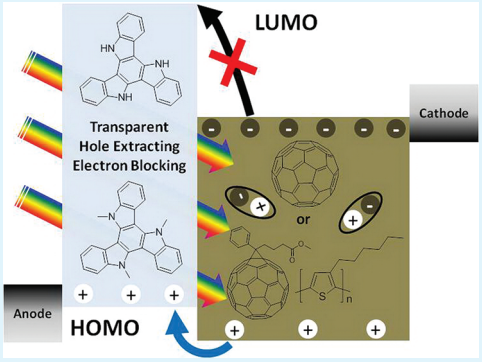

KEYWORDS: *triindoles, organic solar cells, solution processable, hole selective layer, electron blocking*

INTRODUCTION

Organic solar cells (OSCs), as promising low-cost solar energy conversion systems, have experienced significant development in recent decades with the power conversion efficiency increasing from ∼1% to more than 8%.[1−11] This impressive progress has primarily relied on the development of functional materials, device architectures, and morphology control. Of particular interest in the field of organic solar cells is the development of new photoactive materials from small molecule organic semiconductors to conjugated polymers.[12−20] More recently, interface materials have attracted great attention due to the need for highly efficient and stable OSC devices and modules.[21−58]

As a critical component of OSCs located between the photoactive layer and electrodes, a desired interfacial layer should demonstrate a number of functions, i.e., the ability to (1) improve the compatibility of the electrodes and organic active layers, (2) adjust the energy barriers for efficient charge extraction, (3) form a selective contact for one kind of carrier, (4) prevent chemical or physical interactions between the electrodes and photoactive layers, and (5) act as an optical spacer.[21,22] Significant amounts of p- and n- type interface materials have been investigated, including metal oxides, graphene oxides, salts, self assembled organic monolayers and doped conductive polymers.[23−58] Among these, poly(3,4-ethylenedioxythiophene):poly(styrenesulfonate) (PEDOT:PSS) has been one of the most commonly used interlayers on hole-collection electrodes, providing a smooth anode surface, reducing the leakage current, and enhancing device stability compared to a bare electrode.[23] However, it is not an ideal hole selective layer because of several issues, such as its intrinsic acidity and hygroscopicity imposing significant problems in device stability and degradation, and its low LUMO level and bandgap, resulting in weak electron blocking and strong exciton quenching. To replace the problematic PEDOT:PSS, researchers have identified various hole selective materials for OSCs with improved device performance, which include metal oxides, such as nickel oxide (NiOx),[24] molybdenum oxide (MoO_3),[25] and vanadium oxide (V_2O_5),[26] as well as organic semiconductors such as tris[4-(5-phenylthiophen-2-yl)phenyl]amine (TPTPA),[27] 4,4′,4″-tris[N-(3-methylphenyl)-N-phenylamino]triphenylamine (MTDATA),[28] and dithiapyrannylidenes (DITPY).[29] High vacuum processing has been the method of deposition for most of these materials, which is generally believed to be less cost-efficient than solution processing. To our best knowledge, little has been reported on OSCs with solution processed p-type organic interface materials, especially with small molecules.[30,31]

Received: February 9, 2012
Accepted: April 12, 2012
Published: April 12, 2012

Herein, we report our studies on two p-type triindoles, triazatruxene (TAT), and N-trimethyltriindole (TMTI), as solution processable hole selective materials for use in OSCs with bilayer and inverted structures. Owing to their unique discotic π-extended aromatic structure, these C_3 symmetric fused carbazole trimers and their derivatives possess attractive physical and electronic properties for organic electronic devices, e.g. liquid crystallinity, strong fluorescence, and high carrier mobility.[59−70] In addition to these properties, our investigation of TAT and TMTI as hole selective materials is also motivated by their facile preparation, high solubility, electrode compatibility, wide bandgap with good transparency in the visible region, high LUMO (lowest unoccupied molecular orbital) energy level, and modest HOMO (highest occupied molecular orbital) level.

EXPERIMENTAL SECTION

Materials and Instrumentation. Triazatruxene(TAT) and N-trimethyltriindole(TMTI) were synthesized and purified following the procedures reported in the literature.[71] Detailed synthesis and characterization information can be found in the Supporting Information. Pre-patterned ITO-coated glass substrates were purchased from Thin Film Devices Inc. Poly(3-hexylthiophene) (P3HT) was purchased from Rieke Metals, Inc. Phenyl-C61-butyric acid methyl ester (PCBM) was purchased from Nano-C Inc. Sublimed grade C60 and Bathocuproine (BCP) were purchased from Aldrich. PEDOT:PSS (Baytron PH 500) was purchased from H.C. Starck.

Thin film absorption was measured with a CARY 5000 UV-Vis-NIR spectrophotometer. The thickness of these films was determined with a Dektak 150 profilometer. Atomic force microscopy (AFM) images were taken on a Veeco Nanoscope V scanning probe microscope in tapping-mode. Cyclic voltammetry was performed with a Solartron 1285 potentiostat with a scan rate of 100 mV s^{-1}, wherein a platinum wire acts as the counter electrode, glassy carbon as the working electrode, a silver wire acts as the reference electrode. Samples were prepared in dichloromethane solution with 0.1M tetrabutylammoniumhexafluorophosphate as the electrolyte, and ferrocene was used as an internal standard. Density functional theory (DFT) calculations were performed with the Spartan'08 software package using the B3LYP hybrid functional and the 6-31*G basis set to investigate the electronic properties of the materials. The orbital energy levels in vacuum, minimum energy conformations, and electron density plots are recorded.

Device Fabrication and Testing. Photovoltaic devices were fabricated in both the conventional and inverted device configuration. Simple planar heterojunction (bilayer) solar cells were fabricated with a device structure of ITO/PEDOT:PSS (40 nm)/ TAT or TMTI (~3 nm)/ C60 (32 nm)/ BCP (8 nm)/ Ag (100 nm). ITO-coated glass substrates (15 Ω sq^{-1}) were cleaned with detergent, deionized water, acetone, and isopropyl alcohol then dried in an oven at 140 °C for 10 min. Substrates were then treated with UV-ozone for 10 min and coated with PEDOT:PSS with a spin speed of 4000 rpm. The substrates were then baked at 140°C for 20 min to remove the solvent and transferred into the glove box for the remaining processing steps. TAT and TMTI films were spun from a 4 mg/mL solution in methanol and dichlorobenzene, respectively. The thickness of these films was determined with a Dektak 150 profilometer. Both solutions were filtered with a 0.45 μm polytetrafluorethylene filter prior to spin coating at 2000 rpm for 40 sec. C60, BCP, and Ag were thermally evaporated under high vacuum (~2 × 10^{-6} mbar) at a rate of 1.5 Å s^{-1}, 1.5 Å s^{-1}, and 4 Å s^{-1}, respectively. The devices were subsequently annealed at 120 °C for 10 min.

For inverted devices, titania coated ITO films were prepared. First, ITO substrates were cleaned following the method described above. The titania solution was prepared by mixing 200 ml absolute ethanol (Aldrich) with 5 ml ultrapure water and 2 ml concentrated HCl (37.5%). We then mixed titanium ethoxide with this solution in 1:8 ratio. The aforementioned solution of titanium ethoxide diluted in ethanol/water/HCl was spun onto ITO at 2000 rpm to give a film of ~70 nm. The films were annealed at 450 °C for 2 h to promote the growth of the anatase crystalline phase (see the Supporting Information). These films were then cleaned in the solvents mentioned above before being UV-ozoned cleaned again for 10 min. The active layer was spun from a 20 mg mL^{-1} solution of P3HT:PCBM (1:.6 wt %) in dichlorobenzene at 1000 rpm for 60 s in a nitrogen-filled glovebox. The TAT electron blocking layer was spun from a 2 mg/mL solution (in methanol) at 2000 rpm for 40 s. All solutions were passed through a 0.45 μm polytetrafluorethylene filter prior to spin coating. The thicknesses of all films were determined with a Dektak 150 profilometer. Subsequently, Au (50 nm) was thermally evaporated under high vacuum (~ 2 × 10^{-6} mbar) at a rate of 2 Å s^{-1}.

All devices were tested at room temperature in a nitrogen environment under AM 1.5G solar illumination at 100 mW cm^{-2} (1 sun) using a Thermal-Oriel 300W solar simulator with filter and a Keithley 236 source-measure unit for current density-voltage curves. External quantum efficiency (EQE) was measured with a monochromator and calibrated with a silicon diode.

RESULTS AND DISCUSSION

Physical Properties. UV−Vis−NIR spectroscopy was used to evaluate the absorption of the solution processed thin films of TAT and TMTI as shown in Figure 1a. The absorption was

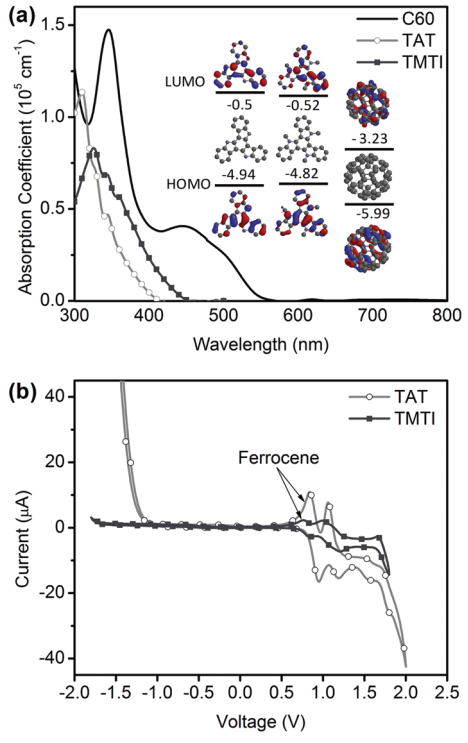

Figure 1. (a) Absorption spectra of solution processed thin films of TAT and TMTI, and vapor deposited C60 film, the inset shows orbital energy levels in vacuum, minimum energy conformations, and electron density plots by DFT calculations; (b) cyclic voltammetry curves of TAT and TMTI in dichloromethane solution with ferrocene as internal reference.

observed mainly in the ultraviolet (UV) region for both films, suggesting high optical bandgaps with excellent transparency in the visible region. Based on the absorption edges, we estimated the optical bandgaps to be ~3.35 eV for TAT and ~3.05 eV for TMTI respectively. Cyclic voltammetry was used to determine the redox properties and then the energy levels of TAT and TMTI. The first oxidation potentials were observed at ~0.23

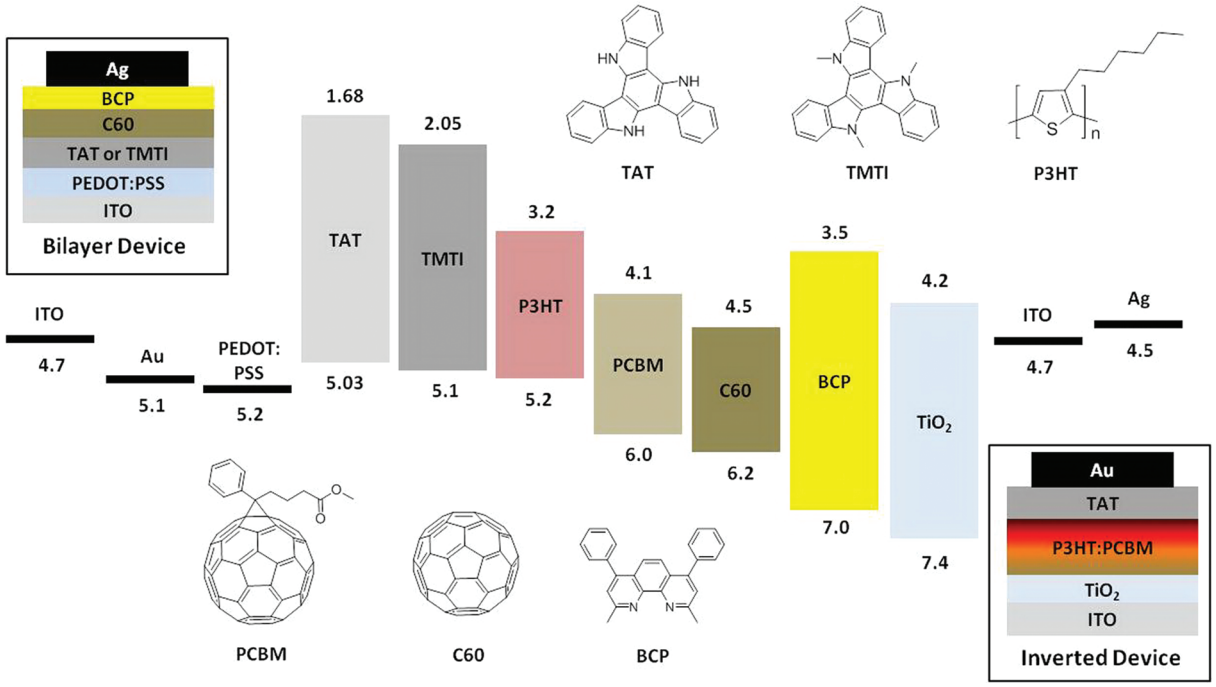

Figure 2. Chemical structures and energy levels of materials used in this study; schematic device structures of bilayer and inverted devices.

and ~0.30 V (vs. ferrocene, −4.8 eV with respect to zero vacuum level)[72] for TAT and TMTI respectively (Figure 1b), which correspond to HOMO levels of −5.03 and −5.1 eV. No reduction peaks were observed within the scan range, consistent with their electron rich nature. The LUMO levels were estimated based on the bandgaps and HOMO levels, which yielded values of −1.68 and −2.05 eV for TAT and TMTI, respectively. Figure 2 shows the schematic energy levels of these molecules together with others materials used in our study.[73] Both TAT and TMTI have high LUMO levels, allowing for efficient electron blocking, while the HOMO levels provide suitable energy levels for hole transfer. DFT calculations were also performed with results shown in the inset of Figure 1a, exhibiting good agreement with the experimental results. According to the energy level alignment in Figure 2, not much of an energetic barrier is expected for hole transfer between these molecules and the electrode.

Thin film topology was characterized by atomic force microscopy (AFM). Figure 3 shows the AFM images for the solution processed thin films on top of PEDOT:PSS before and after thermal annealing at 120 °C for 10 minutes. It was found that both molecules could form continuous films via solution processing, with a root-mean-square (rms) roughness of ~1.3 nm for TAT and ~0.4 nm for TMTI. The TAT film showed more crystalline features than TMTI,[74] which is likely due to the flatter molecular shape of TAT resulting in stronger intermolecular $\pi-\pi$ interactions. (see the Supporting Information) Thermal annealing at 120 °C for 10 min was found to have little-to-no impact on the surface roughness, which prevented the device breakdown by film cracking. Hole carrier mobility of TAT and TMTI films was evaluated by space-charge-limited-current (SCLC) measurements (see Supporting Information), which yielded values of ~1×10^{-4} to 1×10^{-3} $cm^2\ V^{-1}\ s^{-1}$ for both films, enough for efficient hole transport in organic solar cells.

Bilayer Solar Cells. We have tested the hole extracting/electron blocking capability of TAT and TMTI in devices with

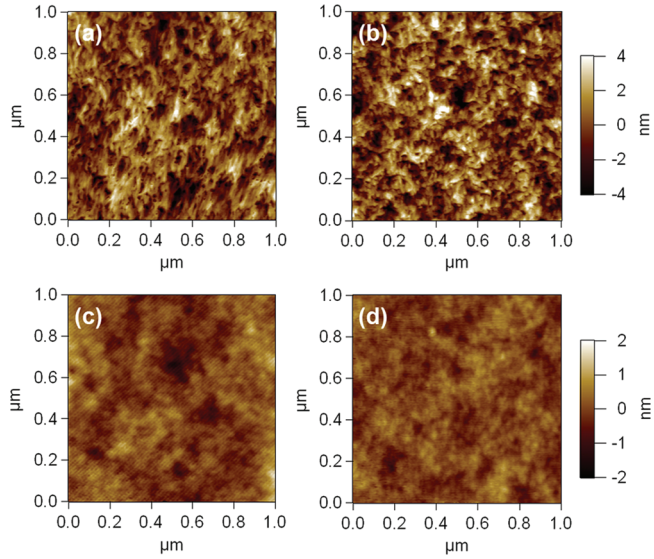

Figure 3. Tapping mode AFM topographical images of solution-processed (a, b) TAT and (c, d) TMTI on top of PEDOT:PSS (a, c) before and (b, d) after thermal annealing at 120 °C for 10 minutes.

a simple planar heterojunction architecture, ITO/PEDOT:PSS/TAT (or TMTI)/ C60 (32 nm)/ BCP (8 nm)/ Ag (100 nm) as shown in Figure 2. A device without the TAT (or TMTI) layer was fabricated as a control. PEDOT:PSS was used in our devices to enable better film uniformity across the ITO substrates. Spin-casting a TAT layer on the top of bare ITO without the PEDOT:PSS layer yielded fewworking devices due to the non-uniform coverage, although those working ones showed similar efficiency as compared to those with PEDOT:PSS (see the Supporting Information). Because of its weak absorption in the visible region (Figure 1a), light harvesting and exciton generation in the TAT (or TMTI) layer is very limited. In the other words, all the bilayer devices tested

here were expected to have excitons generated mainly in the C60 layer and undergo charge separation at the interfaces via hole transfer, instead of electron transfer occurring in typical planar heterojunction devices with excitons generated in the electron donor layer as shown in Figure 4.[75]

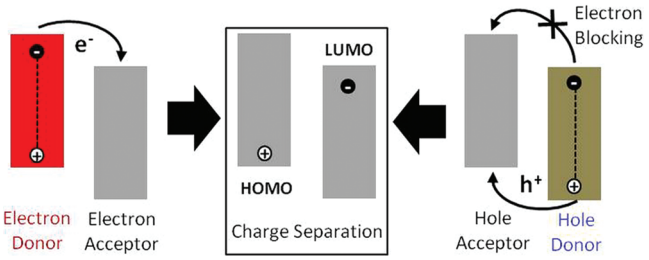

Figure 4. Two types of charge separation in the bilayer donor/acceptor interfaces.

Figure 5 shows the device characteristics for the as-cast devices under AM 1.5 G simulated solar illumination with an intensity of 100 mW cm^{-2}, with values listed in Table 1. The similar shape of the EQE spectra for all three devices confirms that excitons are generated in the C60 layer, provided that the control device has C60 as the sole photoactive layer. It is found that all the device characteristics were enhanced significantly with the addition of a TAT (or TMTI) layer. For instance, power conversion efficiency (PCE) improved from 0.12% to 0.65%; and the external quantum efficiency (EQE) at 450 nm improved from ~12% to greater than 25%. These dramatic improvements were mainly attributed to the superior hole extracting and electron/exciton blocking capabilities of the TAT (or TMTI) layer. First, the large energy gap between the HOMO levels of TAT (or TMTI) at ~5.1 eV and C60 at ~6.2 eV allowed for efficient hole extraction. Secondly, the extremely high LUMO levels (−1.68 eV for TAT and −2.05 eV for TMTI) can easily block electrons from C60 which has a LUMO level of −4.5 eV. This blocking effect is also evidenced by the reduced dark current upon the addition of this TAT (or TMTI) layer as shown in Figure 5b. Thirdly, the hole mobility of the TAT (or TMTI) layer is comparable with the electron mobility of the C60 layer, which ensured sufficient hole/electron balance with reduced charge recombination. Lastly, the high bandgap of TAT (or TMTI) also leads to exciton blocking capability that prevents excitons leakage to the anode.

Further efficiency enhancement has been realized by thermal annealing (see the Supporting Information). Table 1 summarizes the device characteristics of all these devices before and after thermal annealing at 120 °C for 10 min. This improvement is likely attributed to the improved interfaces for better charge separation and reduced charge recombination. The overall efficiency is still much lower than that of state-of-the-art planar heterojunction devices, mainly due to the weak light harvesting capability of the overall device. Nonetheless, a new type of "hole only" device is well presented here, wherein the solar light is mainly harvested by the electron acceptor (or hole donor) layer and efficient exciton dissociation occurs at the interfaces via hole transfer through HOMO levels.

Inverted Solar Cells. We have also investigated the application of TAT as an interfacial layer in inverted solar cells, wherein a typical P3HT:PCBM blend acts as the photoactive layer. The good solubility of TAT in methanol allowed for subsequent deposition of multilayers using

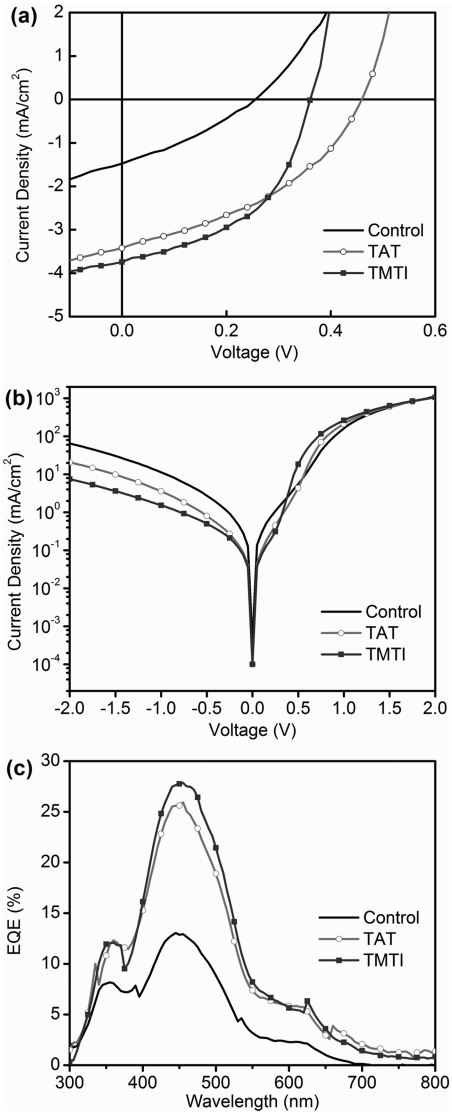

Figure 5. (a) Current density−voltage (J−V) characteristics of bilayer devices with and without TAT or TMTI layer under light, (b) J−V curves of those devices under dark, (c) EQE spectra for those devices.

orthogonal solvents. Specifically, an inverted solar cell with the structure of ITO/TiO_2 (70 nm)/P3HT:PCBM (100 nm)/TAT (< 5 nm)/Au (50 nm) was fabricated, wherein the P3HT:PCBM layer was spun cast in chlorobenzene solution and TAT in methanol solution. The thickness of the TAT layer was controlled by the solution concentration. The best performing device was manufactured by spin-coating a solution of TAT in methanol (2 mg/mL) at 2000 rpm for 40 s. A control device without TAT was built for comparison and the results are displayed in Table 1. It can be found that the addition of the TAT interfacial layer increases the short circuit current from 6.44 to 8.04 mA cm^{-2} by selectively extracting holes and blocking electrons at the Au electrode. This behavior is consistent with a slight rise in V_{oc}, as a result of the decreased recombination.[76] There was not a significant change to the fill factor because such a thin layer of TAT did not substantially affect the ohmicity of the P3HT/Au junction. Overall, the power conversion efficiency increases from 1.06% to 1.34%, a 26% increase. This behavior is again illustrated in the EQE spectrum where the rise is shown mainly from 500−600 nm,

Table 1. Device Performance of Organic Solar Cells under 1 sun AM 1.5 Simulated Illumination[a]

	bilayer devices[a]			inverted devices	
interlayer	N/A	TAT	TMTI	N/A	TAT
V_{oc} (V)	0.26 (0.26)	0.41 (0.47)	0.36 (0.48)	0.41	0.43
J_{sc}(mA/cm2)	1.45 (1.67)	3.28 (3.57)	3.74 (3.89)	6.44	8.04
FF	0.31 (0.37)	0.48 (0.43)	0.48 (0.47)	0.40	0.39
PCE (%)	0.12 (0.16)	0.65 (0.71)	0.65 (0.87)	1.06	1.34

[a]The results in parentheses are for devices annealed at 120 °C for 10 min.

where P3HT:PCBM absorption dominates. Overall, the additional current is not from the light harvesting of TAT, but from improved charge selection in the anode.

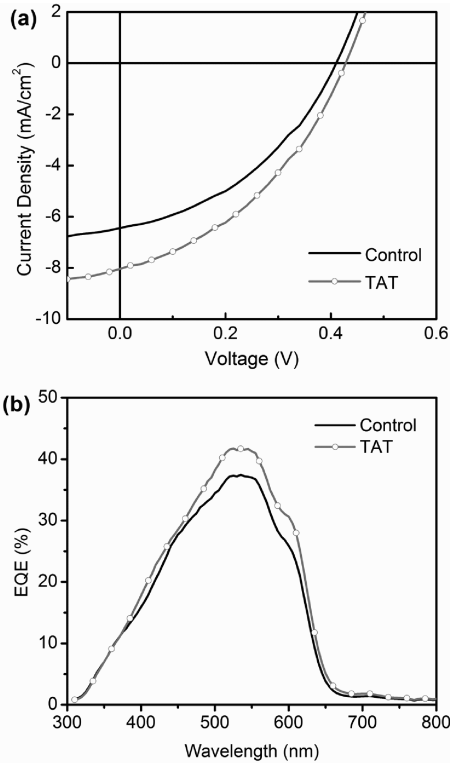

Figure 6. (a) Current density−voltage (J−V) characteristics of inverted devices with and without TAT layer under light, (b) EQE spectra for those devices.

CONCLUSION

In summary, we have synthesized, characterized, and evaluated two solution processable, transparent, organic hole-selective materials, triazatruxene (TAT) and N-trimethyltriindole (TMTI). Their excellent hole extracting and transporting, as well as electron and exciton blocking capabilities were clearly demonstrated in organic solar cells with significantly enhanced device performance. For instance, the insertion of a hole selective layer between PEDOT:PSS and C60 layers in "hole only" planar heterojunction devices increased the power conversion efficiency from 0.16 to 0.71% for TAT and 0.87% for TMTI, respectively. Methanol soluble TAT was also used in an inverted P3HT:PCBM/TiO_2 device, wherein the efficiency improved from 1.06 to 1.34% with the addition of the interlayer. The present results show that triindole-based molecules are highly promising hole selective materials with wide bandgaps, high LUMO levels, modest HOMO levels and high hole mobilities, which can also be easily incorporated into other organic electronic devices. On-going efforts involve the development of various derivatives, such as crosslinkable materials that can be solution processed and converted into insoluble thin films for multilayer structure fabrication; and functionalized materials that can form self-assembled monolayers on electrodes via covalent binding.

ASSOCIATED CONTENT

Supporting Information

Synthesis and characterization of TAT and TMTI, characterization of TiO_2 layer, hole mobility measurements, results for annealed bilayer devices (PDF). This material is available free of charge via internet at http://pubs.acs.org.

AUTHOR INFORMATION

Corresponding Author

*E-mail: BWMa@lbl.gov.

Author Contributions

§These authors contibuted equally to this report.

Notes

The authors declare no competing financial interest.

ACKNOWLEDGMENTS

This work was performed at the Molecular Foundry, Lawrence Berkeley National Laboratory, and was supported by the Office of Science, Office of Basic Energy Sciences, Scientific User Facilities Division, of the U.S. Department of Energy under Contract DE-AC02-05CH11231. S.S. thanks the National Science Foundation for the IGERT Fellowship and the University of California, Berkeley, for the Chancellor's Fellowship.

REFERENCES

(1) Tang, C. W. *Appl. Phys. Lett.* **1986**, *48* (2), 183−185.
(2) Yu, G.; Gao, J.; Hummelen, J. C.; Wudl, F.; Heeger, A. J. *Science* **1995**, *270* (5243), 1789−1791.
(3) Peumans, P.; Uchida, S.; Forrest, S. R. *Nature* **2003**, *425* (6954), 158−162.
(4) Li, G.; Shrotriya, V.; Huang, J. S.; Yao, Y.; Moriarty, T.; Emery, K.; Yang, Y. *Nat. Mater.* **2005**, *4* (11), 864−868.
(5) Ma, W. L.; Yang, C. Y.; Gong, X.; Lee, K.; Heeger, A. J. *Adv. Funct. Mater.* **2005**, *15* (10), 1617−1622.
(6) He, F.; Yu, L. P. *J. Phys. Chem. Lett.* **2011**, *2* (24), 3102−3113.
(7) Beaujuge, P. M.; Frechet, J. M. J. *J. Am. Chem. Soc.* **2011**, *133* (50), 20009−20029.
(8) Chu, T. Y.; Lu, J. P.; Beaupre, S.; Zhang, Y. G.; Pouliot, J. R.; Wakim, S.; Zhou, J. Y.; Leclerc, M.; Li, Z.; Ding, J. F.; Tao, Y. *J. Am. Chem. Soc.* **2011**, *133* (12), 4250−4253.
(9) He, Z. C.; Zhong, C. M.; Huang, X.; Wong, W. Y.; Wu, H. B.; Chen, L. W.; Su, S. J.; Cao, Y. *Adv Mater* **2011**, *23* (40), 4636−4643.

(10) Price, S. C.; Stuart, A. C.; Yang, L. Q.; Zhou, H. X.; You, W. *J. Am. Chem. Soc.* **2011**, *133* (12), 4625−4631.
(11) Wang, M.; Hu, X. W.; Liu, P.; Li, W.; Gong, X.; Huang, F.; Cao, Y. *J. Am. Chem. Soc.* **2011**, *133* (25), 9638−9641.
(12) Kim, B. J.; Miyamoto, Y.; Ma, B. W.; Frechet, J. M. J. *Adv. Funct. Mater.* **2009**, *19* (14), 2273−2281.
(13) Ma, B. W.; Woo, C. H.; Miyamoto, Y.; Frechet, J. M. J. *Chem. Mater.* **2009**, *21* (8), 1413−1417.
(14) Chen, J. J. A.; Chen, T. L.; Kim, B.; Poulsen, D. A.; Mynar, J. L.; Frechet, J. M. J.; Ma, B. W. *ACS Appl. Mater. Interfaces* **2010**, *2* (9), 2679−2686.
(15) Kim, B.; Ma, B. W.; Donuru, V. R.; Liu, H. Y.; Frechet, J. M. J. *Chem. Commun.* **2010**, *46* (23), 4148−4150.
(16) Mauldin, C. E.; Piliego, C.; Poulsen, D.; Unruh, D. A.; Woo, C.; Ma, B. W.; Mynar, J. L.; Frechet, J. M. J. *ACS Appl. Mater. Interfaces* **2010**, *2* (10), 2833−2838.
(17) Zhao, X. Y.; Piliego, C.; Kim, B.; Poulsen, D. A.; Ma, B. W.; Unruh, D. A.; Frechet, J. M. J. *Chem. Mater.* **2010**, *22* (7), 2325−2332.
(18) Chen, T. L.; Chen, J. J. A.; Catane, L.; Ma, B. W. *Org. Electron.* **2011**, *12* (7), 1126−1131.
(19) Chen, T. L.; Zhang, Y.; Smith, P.; Tamayo, A.; Liu, Y.; Ma, B. W. *ACS Appl. Mater. Interfaces* **2011**, *3* (7), 2275−2280.
(20) Leblebici, S. Y.; Catane, L.; Barclay, D. E.; Olson, T.; Chen, T. L.; Ma, B. W. *ACS Appl. Mater. Interfaces* **2011**, *3* (11), 4469−4474.
(21) Steim, R.; Kogler, F. R.; Brabec, C. J. *J. Mater. Chem.* **2010**, *20* (13), 2499−2512.
(22) Ratcliff, E. L.; Zacher, B.; Armstrong, N. R. *J. Phys. Chem. Lett.* **2011**, *2* (11), 1337−1350.
(23) Pingree, L. S. C.; MacLeod, B. A.; Ginger, D. S. *J. Phys. Chem. C* **2008**, *112* (21), 7922−7927.
(24) Irwin, M. D.; Buchholz, B.; Hains, A. W.; Chang, R. P. H; Marks, T. J. *Proc. Natl. Acad. Sci. U.S.A.* **2008**, *105* (8), 2783−2787.
(25) Subbiah, J.; Kim, D. Y.; Hartel, M.; So, F. *Appl. Phys. Lett.* **2010**, *96* (6), 063303.
(26) Li, G.; Chu, C. W.; Shrotriya, V.; Huang, J.; Yang, Y. *Appl. Phys. Lett.* **2006**, *88* (25), 253503.
(27) Kageyama, H.; Ohishi, H.; Tanaka, M.; Ohmori, Y.; Shirota, Y. *Appl. Phys. Lett.* **2009**, *94* (6), 063304.
(28) Zhang, G.; Li, W. L.; Chu, B.; Chen, L. L.; Yan, F.; Zhu, J. Z.; Chen, Y. R.; Lee, C. S. *Appl. Phys. Lett.* **2009**, *94* (14), 143302.
(29) Berny, S.; Tortech, L.; Veber, M.; Fichou, D. *ACS Appl. Mater. Interfaces* **2010**, *2* (11), 3059−3068.
(30) Sun, Y. M.; Gong, X. O.; Hsu, B. B.; Yip, H. L.; Jen, A. K. Y.; Heeger, A. J., *Appl. Phys. Lett.* **2010**, *97* (19), 193310.
(31) Sun, Y. M.; Wang, M. F.; Gong, X. O.; Seo, J. H.; Hsu, B. B. Y.; Wudl, F.; Heeger, A. J. *J. Mater. Chem.* **2011**, *21* (5), 1365−1367.
(32) Rand, B. P.; Li, J.; Xue, J. G.; Holmes, R. J.; Thompson, M. E.; Forrest, S. R. *Adv. Mater.* **2005**, *17* (22), 2714−3718.
(33) Chan, M. Y.; Lee, C. S.; Lai, S. L.; Fung, M. K.; Wong, F. L.; Sun, H. Y.; Lau, K. M.; Lee, S. T. *J. Appl. Phys.* **2006**, *100* (9), 094506.
(34) Khodabakhsh, S.; Sanderson, B. M.; Nelson, J.; Jones, T. S. *Adv. Funct. Mater.* **2006**, *16* (1), 95−100.
(35) Tseng, C. T.; Cheng, Y. H.; Lee, M. C. M. *Appl. Phys. Lett.* **2007**, *91* (23), 233510.
(36) Yip, H. L.; Hau, S. K.; Baek, N. S.; Ma, H.; Jen, A. K. Y. *Adv. Mater.* **2008**, *20* (12), 2376−2382.
(37) Yip, H. L.; Hau, S. K.; Baek, N. S.; Jen, A. K. Y., *Appl. Phys. Lett.* **2008**, *92* (19), 193313.
(38) Hau, S. K.; Yip, H. L.; Acton, O.; Baek, N. S.; Ma, H.; Jen, A. K. Y. *J. Mater. Chem.* **2008**, *18* (42), 5113−5119.
(39) Huang, J. S.; Chou, C. Y.; Liu, M. Y.; Tsai, K. H.; Lin, W. H.; Lin, C. F. *Org. Electron.* **2009**, *10* (6), 1060−1065.
(40) Tao, C.; Ruan, S. P.; Xie, G. H.; Kong, X. Z.; Shen, L.; Meng, F. X.; Liu, C. X.; Zhang, X. D.; Dong, W.; Chen, W. Y., *Appl. Phys. Lett.* **2009**, *94* (4), 043311.
(41) Gao, Y.; Yip, H. L.; Hau, S. K.; O'Malley, K. M.; Cho, N. C.; Chen, H. Z.; Jen, A. K. Y., *Appl. Phys. Lett.* **2010**, *97* (20), 203306.
(42) Gomez, E. D.; Loo, Y. L. *J. Mater. Chem.* **2010**, *20* (32), 6604−6611.
(43) Hains, A. W.; Liu, J.; Martinson, A. B. F.; Irwin, M. D.; Marks, T. J. *Adv. Funct. Mater.* **2010**, *20* (4), 595−606.
(44) Hains, A. W.; Ramanan, C.; Irwin, M. D.; Liu, J.; Wasielewski, M. R.; Marks, T. J. *ACS Appl. Mater. Interfaces* **2010**, *2* (1), 175−185.
(45) Jeon, S. O.; Yook, K. S.; Chin, B. D.; Park, Y. S.; Lee, J. Y. *Sol. Energy Mater. Sol. Cells* **2010**, *94* (8), 1389−1392.
(46) Li, S. S.; Tu, K. H.; Lin, C. C.; Chen, C. W.; Chhowalla, M. *ACS Nano* **2010**, *4* (6), 3169−3174.
(47) Steirer, K. X.; Chesin, J. P.; Widjonarko, N. E.; Berry, J. J.; Miedaner, A.; Ginley, D. S.; Olson, D. C. *Org. Electron.* **2010**, *11* (8), 1414−1418.
(48) Betancur, R.; Maymo, M.; Elias, X.; Vuong, L. T.; Martorell, J. *Sol. Energy Mater. Sol. Cells* **2011**, *95* (2), 735−739.
(49) Hirade, M.; Adachi, C. *Appl. Phys. Lett.* **2011**, *99* (15).
(50) Irwin, M. D.; Servaites, J. D.; Buchholz, D. B.; Leever, B. J.; Liu, J.; Emery, J. D.; Zhang, M.; Song, J. H.; Durstock, M. F.; Freeman, A. J.; Bedzyk, M. J.; Hersam, M. C.; Chang, R. P. H; Ratner, M. A.; Marks, T. J. *Chem. Mater.* **2011**, *23* (8), 2218−2226.
(51) Lassiter, B. E.; Wei, G. D.; Wang, S. Y.; Zimmerman, J. D.; Diev, V. V.; Thompson, M. E.; Forrest, S. R. *Appl. Phys. Lett.* **2011**, *98* (24), 243307.
(52) Murray, I. P.; Lou, S. J.; Cote, L. J.; Loser, S.; Kadleck, C. J.; Xu, T.; Szarko, J. M.; Rolczynski, B. S.; Johns, J. E.; Huang, J. X.; Yu, L. P.; Chen, L. X.; Marks, T. J.; Hersam, M. C. *J. Phys. Chem. Lett.* **2011**, *2* (24), 3006−3012.
(53) Reinhard, M.; Hanisch, J.; Zhang, Z. H.; Ahlswede, E.; Colsmann, A.; Lemmer, U. *Appl. Phys. Lett.* **2011**, *98* (5), 053303.
(54) Salim, T.; Yin, Z. Y.; Sun, S. Y.; Huang, X.; Zhang, H.; Lam, Y. M. *ACS Appl. Mater. Interfaces* **2011**, *3* (4), 1063−1067.
(55) Seo, J. H.; Gutacker, A.; Sun, Y. M.; Wu, H. B.; Huang, F.; Cao, Y.; Scherf, U.; Heeger, A. J.; Bazan, G. C. *J. Am. Chem. Soc.* **2011**, *133* (22), 8416−8419.
(56) Steirer, K. X.; Ndione, P. F.; Widjonarko, N. E.; Lloyd, M. T.; Meyer, J.; Ratcliff, E. L.; Kahn, A.; Armstrong, N. R.; Curtis, C. J.; Ginley, D. S.; Berry, J. J.; Olson, D. C. *Adv. Energy Mater.* **2011**, *1* (5), 813−820.
(57) Zilberberg, K.; Trost, S.; Meyer, J.; Kahn, A.; Behrendt, A.; Lutzenkirchen-Hecht, D.; Frahm, R.; Riedl, T. *Adv. Funct. Mater.* **2011**, *21* (24), 4776−4783.
(58) Zilberberg, K.; Trost, S.; Schmidt, H.; Riedl, T. *Adv. Energy Mater.* **2011**, *1* (3), 377−381.
(59) Feng, G. L.; Lai, W. Y.; Ji, S. J.; Huang, W. *Tetrahedron Lett.* **2006**, *47* (39), 7089−7092.
(60) Lai, W. Y.; Zhu, R.; Fan, Q. L.; Hou, L. T.; Cao, Y.; Huang, W. *Macromolecules* **2006**, *39* (11), 3707−3709.
(61) Gomez-Lor, B.; Alonso, B.; Omenat, A.; Serrano, J. L. *Chem. Commun.* **2006**, No. 48, 5012−5014.
(62) Gomez-Lor, B.; Hennrich, G.; Alonso, B.; Monge, A.; Gutierrez-Puebla, E.; Echavarren, A. M. *Angew. Chem., Int. Ed.* **2006**, *45* (27), 4491−4494.
(63) Garcia-Frutos, E. M.; Gomez-Lor, B. *J. Am. Chem. Soc.* **2008**, *130* (28), 9173−9177.
(64) Talarico, M.; Termine, R.; Garcia-Frutos, E. M.; Omenat, A.; Serrano, J. L.; Gomez-Lor, B.; Golemme, A. *Chem. Mater.* **2008**, *20* (21), 6589−6591.
(65) Lai, W. Y.; He, Q. Y.; Chen, D. Y.; Huang, W. *Chem. Lett.* **2008**, *37* (9), 986−987.
(66) Garcia-Frutos, E. M.; Gutierrez-Puebla, E.; Monge, M. A.; Ramirez, R.; de Andres, P.; de Andres, A.; Ramirez, R.; Gomez-Lor, B. *Org. Electron.* **2009**, *10* (4), 643−652.
(67) Zhao, B. M.; Liu, B.; Png, R. Q.; Zhang, K.; Lim, K. A.; Luo, J.; Shao, J. J.; Ho, P. K. H.; Chi, C. Y.; Wu, J. S. *Chem. Mater.* **2010**, *22* (2), 435−449.
(68) Bura, T.; Leclerc, N.; Fall, S.; Leveque, P.; Heiser, T.; Ziessel, R. *Org. Lett.* **2011**, *13* (22), 6030−6033.
(69) Garcia-Frutos, E. M.; Omenat, A.; Barbera, J.; Serrano, J. L.; Gomez-Lor, B. *J. Mater. Chem.* **2011**, *21* (19), 6831−6836.

(70) Gallego-Gomez, F.; Garcia-Frutos, E. M.; Villalvilla, J. M.; Quintana, J. A.; Gutierrez-Puebla, E.; Monge, A.; Diaz-Garcia, M. A.; Gomez-Lor, B. *Adv. Funct. Mater.* **2011**, *21* (4), 738−745.
(71) Franceschin, M.; Ginnari-Satriani, L.; Alvino, A.; Ortaggi, G.; Bianco, A. *Eur. J. Org. Chem.* **2010**, No. 1, 134−141.
(72) D'Andrade, B. W.; Datta, S.; Forrest, S. R.; Djurovich, P.; Polikarpov, E.; Thompson, M. E. *Org. Electron.* **2005**, *6* (1), 11−20.
(73) Brown, T. M.; Kim, J. S.; Friend, R. H.; Cacialli, F.; Daik, R.; Feast, W. J. *Appl. Phys. Lett.* **1999**, *75* (12), 1679−1681.
(74) Wei, G. D.; Lunt, R. R.; Sun, K.; Wang, S. Y.; Thompson, M. E.; Forrest, S. R. *Nano Lett.* **2010**, *10* (9), 3555−3559.
(75) Zhou, T. L.; Jia, T.; Kang, B. N.; Li, F. H.; Fahlman, M.; Wang, Y. *Adv. Energy Mater.* **2011**, *1* (3), 431−439.
(76) Perez, M. D.; Borek, C.; Forrest, S. R.; Thompson, M. E. *J. Am. Chem. Soc.* **2009**, *131* (26), 9281−9286.